Rapid Communications

Importance of orbital fluctuations for the magnetic dynamics in the heavy-fermion compound SmB_6

Christopher N. Singh* and Wei-Cheng Lee†
Department of Physics, Applied Physics and Astronomy, Binghamton University, Binghamton, New York 13902, USA

(Received 9 April 2018; published 14 June 2018)

The emergent dynamical processes associated with magnetic excitations in heavy-fermion SmB_6 are investigated. By imposing multiorbital interactions on a first-principles model, we find the interplay between spin and orbital fluctuations in the f manifold is highly sensitive to local correlations. The magnetic phase diagram constructed at zero temperature reveals quantum critical features with the existence of several competing phases. Within the random phase approximation, we perform a comprehensive study of the spin-spin correlation function, and our results agree with neutron scattering experiments. Spectral weight analysis shows the low-energy spin excitations are selectively accompanied by orbital fluctuations, indicating a nontrivial entanglement between the spin and orbital degree of freedom driven by relativistic couplings.

DOI: 10.1103/PhysRevB.97.241107

Introduction. While the possibility that SmB_6 is topologically nontrivial has driven many recent efforts [1–12], an equally relevant aspect of this material has been brought to light through the lens of inelastic magnetic neutron scattering (INS). Specifically, the temperature activated [13] dynamical magnetic response signatures observed deep within the insulating state are not traditional magnons, show a high degree of momentum space anisotropy, and have been attributed to correlation driven exciton [14–16] modes. The narrow gap, strong Coulomb interaction, and residual specific heat give exciton-type modes considerable plausibility in the context of this system [17], and identifying the extent to which these excitations contribute to the low-energy transport properties, as well as the interplay between correlation and topology is crucial in understanding SmB_6. In fact, it is well known in the heavy fermions that the Coulomb interaction, lattice geometry, and spin orientation are essential in spawning exotic phenomena; however, fair treatment of the multiorbital nature is often hindered by an exponential growth in complexity. It is precisely this interplay of competing energy scales and many degrees of freedom that invoke the striking electronic properties, yet in spite of this, a multiorbital, first-principles study of the magnetic dynamics in SmB_6 is still lacking.

We address this gap with a realistic model based on complementing density functional theory (DFT) with the generalized random phase approximation (GRPA). This is achieved by projecting the relativistic eigenstates of the Kohn-Sham equations onto Wannier functions, and imposing the multiorbital Hubbard-Kanamori interaction onto these maximally localized orbitals. This approach treats the spin-orbit coupling, multiorbital Coulomb interaction, and band-structure effects on equal footing. Quantum critical features are found at zero temperature with several nearby magnetic phases. In the normal state at finite temperature, the low-energy spin excitations are shown to be tightly coupled to orbital exchange processes through the large spin-orbit coupling, and a number of important features observed in the INS experiments naturally emerge with this approach.

Model. Motivated to capture hybridization effects between localized Sm $4f$ moments, and itinerant Sm $5d$ states, we employ a relativistic multiorbital Hamiltonian as

$$H = H_t + H_{\mathrm{int}}, \tag{1}$$

where H_t is given by

$$H_t = \frac{1}{2}\sum_{ij\alpha\beta\sigma}\left(t_{ij}^{\alpha\beta} - 2\mu\delta_{ij}\delta_{\alpha\beta}\right)c_{i\alpha\sigma}^{\dagger}c_{j\beta\sigma}. \tag{2}$$

Here the fermion operators create (destroy) particles at site i (j), with orbital character α (β) and spin σ. Symmetry considerations and the spin-orbit interaction dictate the Wannier basis is chosen as spinors of the Sm d-eg states and the full Sm f level multiplet [18]. In this way, contained within H_t is the fully relativistic *ab initio* information pertaining to the entirety of the d-f hybridization, as well as f level character in the vicinity of the Fermi energy. This approach has the advantage of treating the f manifold relativistically in contrast to previous studies [15], and is known to be sufficient in producing the hybridization gap [19].

$$\begin{aligned} H_{\mathrm{int}} = {} & \frac{U}{2}\sum_{i\alpha\sigma} n_{i\alpha\sigma}n_{i\alpha\sigma'} \\ & + \sum_{i,\alpha<\beta,\sigma}\{(U-2J)n_{i\alpha\sigma}n_{i\beta\sigma'} + (U-3J)n_{i\alpha\sigma}n_{i\beta\sigma} \\ & + J(c_{i\alpha\sigma}^{\dagger}c_{i\beta\sigma}c_{i\beta\sigma'}^{\dagger}c_{i\alpha\sigma'} - c_{i\alpha\sigma}^{\dagger}c_{i\beta\sigma}c_{i\alpha\sigma'}^{\dagger}c_{i\beta\sigma'})\}. \end{aligned} \tag{3}$$

H_{int} is the centrosymmetric representation [20] of the multiorbital Hubbard-Kanamori interaction [21] that is treated at the mean-field level to calculate the magnetic phase diagram, and at the RPA level to calculate the dynamical spin susceptibility in the normal state. U is the intraorbital repulsion, and J is the Hund's coupling parameter. The first-principles calculations are performed with full potential linear augmented plane waves

*csingh5@bighamton.edu;
http://www.linkedin.com/in/csingh5binghamton/.
†wlee@binghamton.edu;
http://bingweb.binghamton.edu/wlee/.

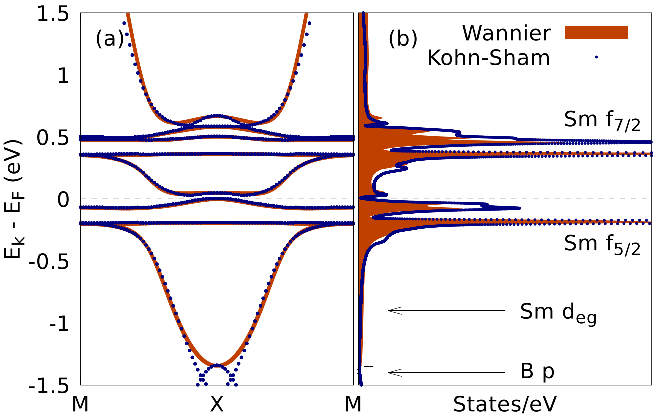

FIG. 1. Electronic structure plots contrasting local-density approximation and Wannier projection. (a) Band structure; (b) density of states.

plus local orbitals and the local-density approximation implemented in the WIEN2K [22] ecosystem. The total energy was converged to 0.1 meV on a 5000 k-point grid with an $RK_{\max}$ of 5. Projection onto Wannier states including fourth nearest neighbors is accomplished with the WANNIER90 package [23], resulting in 40 500 complex hopping parameters.

Figure 1 overlays the Wannier interpolated electronic structure with the Kohn-Sham result. The density of states shows the sharp Sm f peaks with the doubly split $J = 5/2$ and triply split $J = 7/2$ multiplets just below and above the Fermi level, respectively [18]. This electronic structure is representative of O_h point group symmetry in a weak cubic field and strong spin-orbit coupling scheme [24]; in this respect it is commensurate with the latest tunneling spectra [25]. The itinerant Sm d-eg bands are seen to hybridize with the localized f manifold developing a 15 meV direct gap. Excellent agreement is found between the Wannier projection and Kohn-Sham result in the low-energy window $E_f \pm 500$ meV. Admittedly, a parity crossing between the hybridized samarium $4f$ band and the boron p state at the X point lost in this Wannier projection, likely resulting in a shift of the Berry phase. However, being interested in excitation effects, this truncated basis serves as an effective representation of the low-energy physics.

Mean-field theory. Decoupling the quartic terms in the interaction is accomplished as in Refs. [26,27] with

$$\langle c_{i\alpha\sigma}^{\dagger} c_{j\beta\sigma'} \rangle = \left[n_{\alpha} + \frac{\sigma}{2} \cos(\mathbf{q} \cdot \mathbf{r_i}) m_{\alpha} \right] \delta_{ij} \delta_{\alpha\beta} \delta_{\sigma\sigma'}. \tag{4}$$

This leads to a momentum space mean-field Hamiltonian

$$H^{MF} = H_t + \sum_{\mathbf{p}\alpha\sigma} \theta_{\alpha} c_{\mathbf{p}\alpha\sigma}^{\dagger} c_{\mathbf{p}\alpha\sigma} + \zeta + \sum_{\mathbf{p}\alpha\sigma} \eta_{\alpha\sigma} (c_{\mathbf{p}\alpha\sigma}^{\dagger} c_{\mathbf{p}+\mathbf{q}\alpha\sigma} + \text{H.c.}) \tag{5}$$

with mean-field potentials

$$\theta_{\alpha} = U n_{\alpha} + (2U - 5J) \sum_{\beta \neq \alpha} n_{\beta},$$

$$\eta_{\alpha\sigma} = -\frac{\sigma}{2} \left(U m_{\alpha} + J \sum_{\beta \neq \alpha} m_{\beta} \right) \tag{6}$$

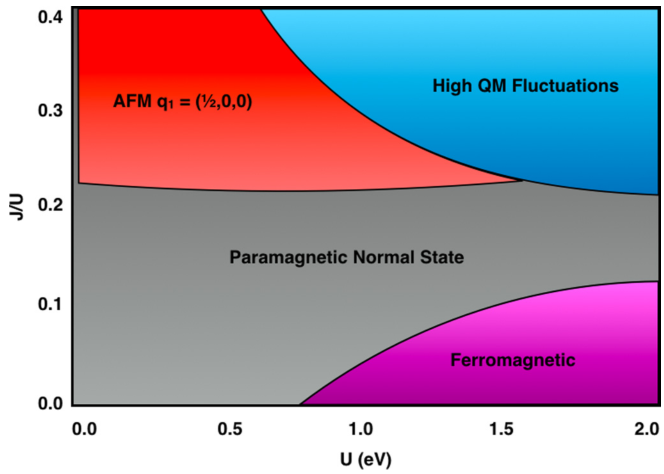

FIG. 2. Schematic magnetic phase diagram of SmB_6 obtained by mean-field treatment of first-principles Wannier projection.

and mean-field constant

$$\zeta = \frac{J}{2} \sum_{\alpha \neq \beta} m_{\alpha} m_{\beta} - U \sum_{\alpha} \left(n_{\alpha}^2 - \frac{1}{4} m_{\alpha}^2 \right) - (2U - 5J) \sum_{\alpha \neq \beta} n_{\alpha} n_{\beta}. \tag{7}$$

Calculating the phase diagram proceeds by self-consistently determining the mean-field parameters n_{α} and $m_{\alpha} = n_{\alpha\uparrow} - n_{\alpha\downarrow}$, with convergence characterized by $\| D \| < 1 \times 10^{-5}$.

$$D = \langle n_{i+1}^{\alpha} - n_i^{\alpha} | \frown \langle m_{i+1}^{\alpha} - m_i^{\alpha} |. \tag{8}$$

Minimization of the norm of D gives the self-consistent condition, automatically ensuring a minimum in the free energy [28]. The self-consistent process is repeated across different magnetic phases and ordering wave vectors. We consider a set of five phases characterized by three antiferromagnetic ordering wave vectors $\mathbf{q}_1 = (\frac{1}{2},0,0)$, $\mathbf{q}_2 = (\frac{1}{2},\frac{1}{2},0)$, $\mathbf{q}_3 = (\frac{1}{2},\frac{1}{2},\frac{1}{2})$, and the paramagnetic and ferromagnetic phases. The total particle number is constrained to the experimental average Sm valence of 2.54 [29] during each of the self-consistency cycles.

Figure 2 shows the zero temperature magnetic phase diagram in the plane of the interaction parameters U and J. A central feature consistent with muon spin rotation (μSR) experiments [30] is the large paramagnetic belt found in the region with moderate correlations where the intraorbital repulsion is comparable to the f level bandwidth W. Interestingly, in the regime of large Hund's coupling J compared to intraorbital repulsion U, $\mathbf{q}_1 = (\frac{1}{2},0,0)$ antiferromagnetic order is found to be the ground state. We notice that high-pressure experiments [31] have already seen evidence for this one-dimensional- (1D) like antiferromagnetic order, and a recent theoretical study reported in Ref. [32] has obtained similar results. The region of $U > 1$ eV, $J/U > 1/5$ shows several phases very close in energy, suggesting the dominance of quantum fluctuations and highly competing order. For $U \gg J/U$, ferromagnetism is found to be the lowest-energy magnetic phase. It is worth mentioning that experimental evidence for ferromagnetic order is not conclusive. While μSR experiments [30] find no evidence of long-range ferromagnetic order, magnetoresistance experiments [33] are suggestive of ferromagnetic puddling. In short, our mean-field calculations are commensurate with experiments in suggesting a system with various competing magnetic orders at zero temperature, implying the magnetic dynamics are complicated even in the normal state at finite temperatures.

Spin susceptibility. In order to deepen our understanding of the spin dynamics in multiorbital spin-orbit coupled systems, we study the magnetic excitations in the normal state with the following correlation tensor:

$$\mathring{\chi}^{\gamma\delta}_{\alpha\alpha'\beta\beta'}(\mathbf{q},i\omega_n) = \int_0^\beta d\tau\, e^{i\omega_n\tau}\langle T_\tau m^\gamma_{\alpha\alpha'}(\mathbf{q},\tau) m^\delta_{\beta\beta'}(-\mathbf{q},0)\rangle, \quad (9)$$

where, for example,

$$m^z_{\alpha\alpha'}(\mathbf{q},\tau) = \sum_{\mathbf{p}\sigma} \sigma c^\dagger_{\mathbf{p}+\mathbf{q}\alpha\sigma}(\tau) c_{\mathbf{p}\alpha'\sigma}(\tau). \quad (10)$$

The subscript greek indices represent orbitals and the superscript indices represent magnetization direction components. Evaluation of the correlation tensor follows textbook procedures [34], and the bare susceptibility can be expressed by the generalized Lindhard function

$$\begin{aligned} \mathring{\chi}^{zz}_{\bar\alpha\bar\beta}(\mathbf{q},\omega) &= \frac{1}{2N}\sum_{\mathbf{p}\sigma} \sigma\, \Xi^{ab\sigma}_{\bar\alpha\bar\beta}(\mathbf{p},\mathbf{q}) \Lambda_{ab}(\mathbf{p},\mathbf{q},\omega), \\ \Xi^{ab\sigma}_{\bar\alpha\bar\beta}(\mathbf{p},\mathbf{q}) &\equiv \left(U^{\mathbf{p}+\mathbf{q}}_{\alpha a\sigma}\right)^* U^{\mathbf{p}}_{\alpha' b\sigma} \left(U^{\mathbf{p}}_{\beta b\sigma}\right)^* U^{\mathbf{p}+\mathbf{q}}_{\beta' a\sigma}, \\ \Lambda_{ab}(\mathbf{p},\mathbf{q},\omega) &\equiv \frac{n_F(\xi_{\mathbf{p}+\mathbf{q}a}) - n_F(\xi_{\mathbf{p}b})}{\omega + i\eta + \xi_{\mathbf{p}b} - \xi_{\mathbf{p}+\mathbf{q}a}}, \end{aligned} \quad (11)$$

where contravariant indices are eigenbasis indices and are summed over, Ξ is the orbital projection weight, and Λ gives the thermal occupations. Here the rank-four tensor is operated as a matrix by defining the sets $\bar\alpha = \{\alpha,\alpha'\}$ and $\bar\beta = \{\beta,\beta'\}$. Due to the presence of strong spin-orbit coupling, the longitudinal (χ^{zz}) and transverse ($\chi^{\pm}$) functions are calculated separately since they could be different. Within the GRPA, the renormalized correlation functions become

$$\begin{aligned} \chi^{zz}_{\bar\alpha\bar\beta} &= \chi^1 + \chi^4 - \chi^2 - \chi^3, \\ \chi^{\pm}_{\bar\alpha\bar\beta} &= \chi^5. \end{aligned} \quad (12)$$

The functions $\chi^{1\text{–}5}$, along with the interaction kernel are worked out in great detail in Refs. [35,36]. The spectral function of this correlator is directly measured by INS experiments, and what is known from experiment is the low-energy peaks around 14 meV cannot be attributed to phonon, crystal field, or pure magnon modes [14].

Discussion. To gain insight into the origin of these peaks, we analyze the orbital components of the spectra around 14 meV for a set of scattering vectors tested by Ref. [14]. The GRPA calculations were performed on an 8000 k-point grid in the full Brillouin zone with a thermal broadening factor fixed to $\eta = 0.5$ meV. Table I summarizes how the correlation tensor is used to classify processes depending on initial and final orbital states, and Fig. 3 shows two orbital decompositions of the spectral function extracted via the sum and the trace of the longitudinal function from Eq. (12).

Consider first the bare and the GRPA susceptibilities in Fig. 3(a). The bare function shows no signature at 14 meV, whereas the GRPA produces peaks matching the INS data, indicating these modes are a result of electron correlations instead of wave-vector nestings. Furthermore, the difference between the sum and the trace of the spectral function demonstrates the extent to which spin excitations at that wave vector have considerable orbital content. This is readily visible in comparing Figs. 3(a), 3(b), and 3(d) to Fig. 3(c). If the sum and the trace have nearly identical line shapes, the corresponding peak is mainly associated with spin-flip processes within intraorbital channels. In this case, orbital fluctuations are not coupled to this spin mode despite the strong spin-orbit interaction. On the other hand, if the trace is only a portion of the sum around an INS peak, the corresponding peak carries significant weight in the interorbital channel, and orbital fluctuations are strongly entangled with this spin excitation. Comparing the spin-spin correlation function at all four momenta plotted in Fig. 3, we find that the magnetic excitations at $q = (0,0.695,0.695)$, $(0.98,0.69,0.69)$, and $(0.77,0.26,0.26)$ have large interorbital contributions while those at $q = (0.49,0.49,0.49)$ are mainly in the intraorbital channels. This observation indicates that the effects of the interactions driving the spin collective modes near 14 meV are inhomogeneous throughout the momentum space, despite the fact that SmB_6 has a centrosymmetric crystal structure and the Sm point group should be at lowest D_{4h}. This strongly suggests the orbital degree of freedom plays a crucial role in the collective excitations emerging from electron correlations, and may lead to the symmetry-breaking magnetic response witnessed in Ref. [37], for example.

TABLE I. Sum and trace operations on the correlation tensors as used to determine if orbital fluctuations are present in the excitation channel.

Function	Orbital conservation
$\sum_{\bar\alpha\bar\beta}(\chi^{\pm}_{\bar\alpha\bar\beta})$	No
$\sum_{\bar\alpha\bar\beta}(\chi^{zz}_{\bar\alpha\bar\beta})$	No
$\mathrm{tr}(\chi^{\pm}_{\bar\alpha\bar\beta})$	Yes
$\mathrm{tr}(\chi^{zz}_{\bar\alpha\bar\beta})$	Yes

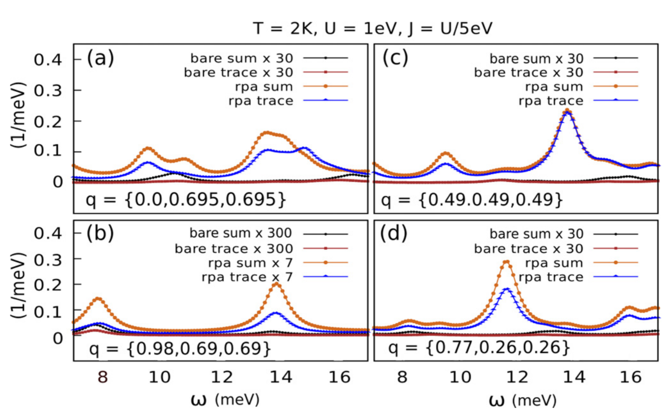

FIG. 3. Longitudinal spin response spectrum for selected scattering vectors of INS data of Ref. [14]. Note the spectra have been scaled differently.

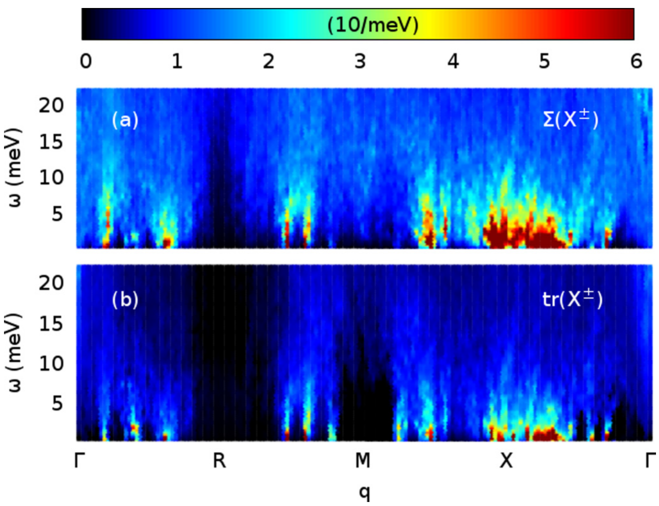

FIG. 4. Top: The sum of the transverse function for $T = 1$ K, $U = 1$ eV, $J = U/10$. Bottom: trace of the transverse function for $T = 1$ K, $U = 1$ eV, $J = U/10$.

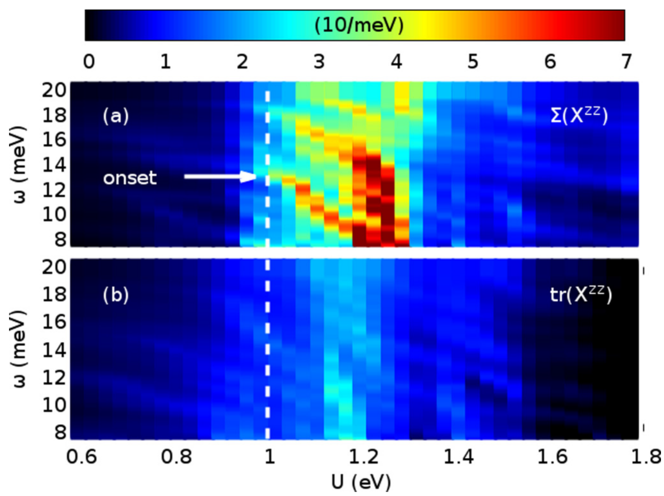

FIG. 5. Scattering at $q = (0,0.695,0.695)$ as a function of interaction for $T = 2$ K, $J = U/5$. (a) The sum of the longitudinal function. (b) The trace of the longitudinal function.

Figure 4 maps the transverse spin excitation in frequency-momentum space. The inter- vs. intraorbital channels can be seen to have different structure and intensity as a function of the scattering wave vector. This reiterates a strong inhomogeneity in the spin-orbital coupling, and supports the idea that the low-energy states are selectively susceptible to orbital excitations. The peak around $\mathbf{q} = X$ observed in INS and in our data can be directly tied to the phase diagram, as this excitation is associated with 1D antiferromagnetic (AFM) order. The lowest-lying excitations exhibiting a reduced dimensionality profile has ramifications on transport properties as discussed by Ref. [17], especially given the centrosymmetry present in the crystal structure and our interaction kernel. The fact that we find the X point susceptibility peaking near 4 meV is indicative that in our model, the cost of the 1D AFM excitation is within 10 meV of experiment. Given the fact we are in a weak-coupling regime, this suggests that even though this is correlation driven physics, the $U \to \infty$ limit is not absolutely necessary. This alleviates chemical potential pinning and integer occupancy constraints imposed by slave bosonization, for example, and is another benefit of this approach to mixed valent systems. To explore this further, the onset of the excitation is studied as a function of local correlations.

Figure 5 shows the longitudinal susceptibility as a function of U with $J = U/5$ for the selected scattering vector $\mathbf{q} = (0,0.695,0.695)$. We find that the excitation at 14 meV onsets as $U \approx W \approx 1$ eV, and is driven down in energy as a function of U. While the result agrees with the previous study [15,16], our results further ascribe significant orbital angular momentum to the spectral weight of the 14 meV mode by comparing the trace and the sum. The trace in Fig. 5(b) showing a significantly weaker excitation profile than the sum in Fig. 5(a), again shows that at this specific wave vector there is significant orbital character in the excitation. In light of the phase diagram in Fig. 2, increasing U drives the system into a region of high fluctuations, reducing the energy cost of instantiating this specific spin-orbital excitation. The fact that the 14 meV peak arises when $U \approx W$ places a strong constraint on theoretical treatment of correlations in SmB_6, further showing the $U \to \infty$ limit is an unnecessary assumption if starting with an accurate electronic dispersion.

Conclusion. We have shown that a first-principles model can reproduce the low-energy physics in SmB_6, and that momentum-dependent entanglement between the spin and orbital degree of freedom emerges naturally from strong spin-orbit coupling. The various competing magnetic phases at zero temperature lead to nontrivial magnetic dynamics in the normal state, and spectral decomposition of the spin susceptibility exposes the anisotropic orbital character of the excitations. This first-principles approach clarifies a number of intriguing features observed in the inelastic neutron scattering measurement. With the evidence presented here, we propose the orbitally degenerate nondispersive f manifold is the perfect environment to harbor *orbital exciton* modes, a new correlation driven mode carrying exclusively orbital angular momentum. This conjecture proffers a different physical interpretation when considering nontrivial topology with a charge-neutral Fermi surface, and provides a simple mechanism for bulk SmB_6 to couple selectively to magnetic perturbations while simultaneously ignoring the charge sector. This exciton form allows an additional pathway for low-temperature specific heat anomalies, and will additionally cause an orbital dichroic signal in optical probes. Further work to address the role of topology, as well as quantitative descriptions of these contemporary exciton modes is underway.

Acknowledgments. This work utilized the Extreme Science and Engineering Discovery Environment (XSEDE) supported by National Science Foundation Grant No. ACI-1548562. It was also supported by a Binghamton University start-up fund. The authors thank Pegor Aynajian for discussions regarding INS and Feliciano Giustino for discussions regarding DFT.

[1] A. Menth, E. Buehler, and T. H. Geballe, Phys. Rev. Lett. **22**, 295 (1969).
[2] L. Kouwenhoven and L. Glazman, Phys. World **14**, 33 (2001).
[3] M. C. Hatnean, M. R. Lees, D. M. Paul, and G. Balakrishnan, Sci. Rep. **3**, 3071 (2013).
[4] M. Dzero, K. Sun, V. Galitski, and P. Coleman, Phys. Rev. Lett. **104**, 106408 (2010).
[5] S. Wolgast, C. Kurdak, K. Sun, J. W. Allen, D.-J. Kim, and Z. Fisk, Phys. Rev. B **88**, 180405 (2013).
[6] D. J. Kim, S. Thomas, T. Grant, J. Botimer, Z. Fisk, and J. Xia, Sci. Rep. **3**, 3150 (2013).
[7] D. J. Kim, J. Xia, and Z. Fisk, Nat. Mater. **13**, 466 (2014).
[8] M. Neupane, N. Alidoust, S. Xu, T. Kondo, Y. Ishida, D.-J. Kim, C. Liu, I. Belopolski, Y. Jo, T.-R. Chang *et al.*, Nat. Commun. **4**, 2991 (2013).
[9] N. Xu, P. K. Biswas, J. H. Dil, R. S. Dhaka, G. Landolt, S. Muff, C. E. Matt, X. Shi, N. C. Plumb, M. Radović *et al.*, Nat. Commun. **5**, 4566 (2014).
[10] N. Wakeham, P. F. S. Rosa, Y. Q. Wang, M. Kang, Z. Fisk, F. Ronning, and J. D. Thompson, Phys. Rev. B **94**, 035127 (2016).
[11] G. Li, Z. Xiang, F. Yu, T. Asaba, B. Lawson, P. Cai, C. Tinsman, A. Berkley, S. Wolgast, Y. S. Eo, D.-J. Kim, C. Kurdak, J. W. Allen, K. Sun, X. H. Chen, Y. Y. Wang, Z. Fisk, and L. Li, Science **346**, 1208 (2014).
[12] B. Tan, Y.-T. Hsu, B. Zeng, M. C. Hatnean, N. Harrison, Z. Zhu, M. Hartstein, M. Kiourlappou, A. Srivastava, M. Johannes *et al.*, Science **349**, 287 (2015).
[13] P. Nyhus, S. L. Cooper, Z. Fisk, and J. Sarrao, Phys. Rev. B **55**, 12488 (1997).
[14] P. Alekseev, J. Mignot, J. Rossat-Mignod, V. Lazukov, I. Sadikov, E. Konovalova, and Y. B. Paderno, J. Phys.: Condens. Matter **7**, 289 (1995).
[15] W. T. Fuhrman and P. Nikolić, Phys. Rev. B **90**, 195144 (2014).
[16] W. T. Fuhrman, J. Leiner, P. Nikolić, G. E. Granroth, M. B. Stone, M. D. Lumsden, L. DeBeer-Schmitt, P. A. Alekseev, J.-M. Mignot, S. M. Koohpayeh, P. Cottingham, W. A. Phelan, L. Schoop, T. M. McQueen, and C. Broholm, Phys. Rev. Lett. **114**, 036401 (2015).
[17] J. Knolle and N. R. Cooper, Phys. Rev. Lett. **118**, 096604 (2017).
[18] C.-J. Kang, J. Kim, K. Kim, J. Kang, J. D. Denlinger, and B. I. Min, J. Phys. Soc. Jpn. **84**, 024722 (2015).
[19] A. Yanase and H. Harima, Prog. Theor. Phys. Suppl. **108**, 19 (1992).
[20] The centrosymmetric approximation is used for simplicity, but some recent evidence [37] suggests that a more detailed treatment of the interorbital interaction may be pertinent.
[21] J. Kanamori, Prog. Theor. Phys. **30**, 275 (1963).
[22] P. Blaha, K. Schwarz, G. Madsen, D. Kvasnicka, and J. Luitz, *WIEN2k, An augmented Plane Wave Plus Local Orbitals Program for Calculating Crystal Properties* (Techn. Universitat Wien, Austria, 2001).
[23] A. A. Mostofi, J. R. Yates, G. Pizzi, Y.-S. Lee, I. Souza, D. Vanderbilt, and N. Marzari, Comput. Phys. Commun. **185**, 2309 (2014).
[24] M. Tinkham, *Group Theory and Quantum Mechanics* (Courier Corporation, North Chelmsford, 2003). p. 79.
[25] Z. Sun, A. Maldonado, W. S. Paz, D. S. Inosov, A. P. Schnyder, J. J. Palacios, N. Y. Shitsevalova, V. B. Filippov, and P. Wahl, Phys. Rev. B **97**, 235107 (2018).
[26] T. Nomura and K. Yamada, J. Phys. Soc. Jpn. **69**, 1856 (2000).
[27] E. Dagotto, A. Moreo, A. Nicholson, Q. Luo, S. Liang, and X. Zhang, Front. Phys. **6**, 379 (2011).
[28] D. D. Johnson, Phys. Rev. B **38**, 12807 (1988).
[29] Y. Utsumi, D. Kasinathan, K.-T. Ko, S. Agrestini, M. W. Haverkort, S. Wirth, Y.-H. Wu, K.-D. Tsuei, D.-J. Kim, Z. Fisk, A. Tanaka, P. Thalmeier, and L. H. Tjeng, Phys. Rev. B **96**, 155130 (2017).
[30] P. K. Biswas, Z. Salman, T. Neupert, E. Morenzoni, E. Pomjakushina, F. von Rohr, K. Conder, G. Balakrishnan, M. C. Hatnean, M. R. Lees, D. M. Paul, A. Schilling, C. Baines, H. Luetkens, R. Khasanov, and A. Amato, Phys. Rev. B **89**, 161107 (2014).
[31] A. Barla, J. Derr, J. P. Sanchez, B. Salce, G. Lapertot, B. P. Doyle, R. Rüffer, R. Lengsdorf, M. M. Abd-Elmeguid, and J. Flouquet, Phys. Rev. Lett. **94**, 166401 (2005).
[32] K.-W. Chang and P.-J. Chen, Phys. Rev. B **97**, 195145 (2018).
[33] Y. Nakajima, P. Syers, X. Wang, R. Wang, and J. Paglione, Nat. Phys. **12**, 213 (2016).
[34] G. D. Mahan, *Many-Particle Physics* (Springer Science & Business Media, Berlin, 2013).
[35] X. Wu, F. Yang, C. Le, H. Fan, and J. Hu, Phys. Rev. B **92**, 104511 (2015).
[36] S. Mukherjee and W.-C. Lee, Phys. Rev. B **94**, 064407 (2016).
[37] Z. Xiang, B. Lawson, T. Asaba, C. Tinsman, L. Chen, C. Shang, X. H. Chen, and L. Li, Phys. Rev. X **7**, 031054 (2017).